



Simulated resumption of the North Atlantic meridional overturning circulation – Slow basin-wide advection and abrupt local convection

M. Renold^a, C.C. Raible^{a,b,*}, M. Yoshimori^{a,1}, T.F. Stocker^{a,b}

^aClimate and Environmental Physics, Physics Institute, University of Bern, 3012 Bern, Switzerland

^bOeschger Centre for Climate Change Research, University of Bern, Switzerland

ARTICLE INFO

Article history:

Received 9 February 2009

Received in revised form

16 October 2009

Accepted 2 November 2009

ABSTRACT

The resumption process of the North Atlantic meridional overturning circulation (MOC) is investigated in a series of freshwater hosing experiments using a comprehensive coupled climate model. Four different freshwater perturbations are applied to the North Atlantic between 50°N and 70°N leading to a substantial weakening of MOC and an expansion of winter sea ice cover over the Greenland–Iceland–Norwegian (GIN) Seas. Deactivating the freshwater forcing leads to a two-phase recovery of the MOC. The first phase is a slow basin-wide advection process whereas the second phase is an abrupt, decadal-scale transition, located in the North Atlantic. The slow basin-wide advection process to an intermediate state of the MOC is characterized by a restart of the deep water production in the area of the subpolar gyre and the Irminger Basin. However, the ice cover over the GIN Seas remains, whereas the surface density gradually increases in the GIN Seas on a century time scale. The length of this intermediate state depends on the strength of freshwater perturbation, which determines the magnitude of the meridional density gradient in the North Atlantic. The second transition phase is triggered by a model-specific density threshold reached in the GIN Seas. When passed, the MOC abruptly intensifies by ~60% within 60–80 years. The analysis shows that this abrupt intensification only depends on surface salinity in the GIN Seas. The model results reveal that the simulated sea ice retreat in the GIN Seas and a rapid increase of the Greenland air temperature of the second phase of the resumption of the MOC are similar in amplitude to temperature proxies observed during Dansgaard–Oeschger events of the last ice age.

© 2009 Elsevier Ltd. All rights reserved.

1. Introduction

A wide range of proxy data shows that several abrupt climate changes occurred during the last ice age and the last termination (Ruddiman and McIntyre, 1981; Dansgaard et al., 1993; Stocker, 2000). These so-called Dansgaard–Oeschger events (D/O) are most likely linked to changes of the North Atlantic meridional overturning circulation (MOC) (Bond et al., 1993; Stocker and Marchal, 2000; Rahmstorf, 2002; McManus et al., 2004). This connection is confirmed by climate models, which are exposed to freshwater discharge perturbations, e.g., Stocker et al. (1992); Manabe and Stouffer (1995); Vellinga and Wood (2002); Schmittner et al. (2003); Knutti et al. (2004); Stouffer et al., (2006).

Building on the seminal investigation of the MOC by Stommel (1961), most of the current modelling studies focus on the rapid

decline of the MOC, changes with respect to a shutdown of the MOC, and the interhemispheric linkages leading to a variety of global climate changes. Such freshwater discharge experiments show that the weakening of the MOC goes along with a reduction of Atlantic Ocean heat transport to higher northern latitudes and is responsible for a distinct ocean and atmosphere temperature decrease in the region of the North Atlantic (Stocker et al., 1992; Rühlemann et al., 1999; Rind et al., 2001; Rahmstorf, 2002; Vellinga and Wood, 2002; Schmittner et al., 2003; Knutti et al., 2004; Vidal et al., 2005). This response of the climate system is not restricted to the Northern Hemisphere. The suppression of deep water formation in the northern North Atlantic causes a southern hemispheric warming, as the northward heat transport is strongly reduced (Stocker, 1998; Stocker and Johnsen, 2003). There is strong proxy evidence from Antarctica indicating such a warming of the Southern Hemisphere (Blunier et al., 1998; EPICA Community Member, 2006; Barker et al., 2009).

However, there are still many uncertainties in climate model simulations. For instance, Stocker et al. (2007) found that the response of the Southern Hemisphere depends on the experimental design, i.e., the application of a salt compensation, and

* Corresponding author at: Climate and Environmental Physics, Physics Institute, University of Bern, Sidlerstr. 5, 3012 Bern, Switzerland. Tel.: +41 31 631 4450.

E-mail address: raible@climate.unibe.ch (C.C. Raible).

¹ Present address: Center for Climate System Research, University of Tokyo, Japan.

a specific parametrization in ocean models representing eddy mixing. Knutti et al. (2000) showed that the stability of the MOC is highly influenced by parametrizations of vertical mixing schemes. Moreover, the MOC depends on the vertical and the horizontal diffusivities (Schmittner and Weaver, 2001; Longworth et al., 2005). All these processes are critical factors determining the characteristics of the dynamical system in terms of a possible shutdown of the MOC but also in terms of a resumption (De Vries and Weber, 2005; Dijkstra, 2005). Additionally, feedback processes like sea-ice brine rejection, freshwater releases in the ventilation areas, the impact of the atmospheric hydrological cycle, and the role of vegetation are identified to be relevant in the stability and temporal behavior of the MOC (Wang, 2005).

Most of the modelling studies concentrate on the climate response due to an MOC shutdown. However, mechanisms that are responsible for the resumption of the MOC are still not fully understood. Clearly, vertical mixing processes in the ocean's interior and wind-induced Ekman upwelling are important mechanisms for MOC variations (Kuhlbrodt et al., 2007). Concerning the former mechanism Wright and Stocker (1991) suggested that a slow warming of the abyssal water destabilizes the stratification of the ocean, and therefore the water column is rapidly reorganized leading to a large heat loss of the ocean. Instead of a warming of the abyssal water Knorr and Lohmann (2003) showed an alternative mechanism affecting the vertical mixing: the MOC rapidly recovers within decades when the surface temperature around Antarctica is steadily increased from glacial to interglacial conditions accompanied by a retreat of the Antarctic sea ice. On the other hand Goosse et al. (2002) used a climate model of reduced complexity and found that the major deep water production areas in the North Atlantic can shift southward in a spontaneous way. This leads to an abrupt reduction of the MOC with associated surface cooling for several hundred years.

Stouffer et al. (2006) showed in a model inter-comparison study on freshwater hosing experiments that a few experiments reveal no resumption of the MOC for a strong freshwater forcing. Most models show a recovery of the MOC, some with a significant overshooting of the MOC by more than 30% compared with the control experiment. Recently, Hu et al. (2008) showed in a series of comprehensive model simulations that the recovery of the MOC strongly depends on the through-flow of the Bering Strait. The recovery is at least a century earlier in an open Bering Strait than if the Bering Strait is closed. Additionally, the change to last glacial maximum (LGM) conditions has no strong effect on the recovery of the MOC compared to a present-day simulation with closed Bering Strait (Hu et al., 2008). The speed of MOC resumption critically depends on the specifics of the freshwater forcing as was shown recently in simulations of the last termination Liu et al. (2009).

Our study enters into this series of MOC resumption studies using a set of sensitivity AOGCM experiments with a freshwater discharge in the North Atlantic. Despite the diversity of feedback processes and possible mechanisms, the MOC is directly linked to buoyancy loss and gain in the area of deep water production. Therefore, we focus our investigation on density changes in the northern North Atlantic, which are mainly driven by salt rather than temperature. The salinity budget in the Greenland–Iceland–Norwegian (GIN) Seas provides a new perspective on the underlying process of the resumption of the MOC.

The outline of this paper is as follows. In Section 2, we introduce the model and the experimental setup. Section 3 presents the climate response of the North Atlantic with respect to the freshwater forcing. We focus on the processes, which are responsible for the resumption of the MOC after the freshwater flux is switched off. Finally, the results are summarized and discussed in Section 4.

2. Model and experimental design

We use the Community Climate System Model (CCSM, version 3.0) developed by the National Center of Atmospheric Research (NCAR) (Collins et al., 2006a; Yeager et al., 2006). This atmosphere–ocean general circulation model (AOGCM) consists of an atmosphere, an ocean, a land, and a sea ice component. A coupler connects the components without flux corrections. The atmospheric model has a spectral resolution of T31, which corresponds to approximately $3.75^\circ \times 3.75^\circ$ in longitude–latitude. It uses 26 hybrid sigma–pressure levels up to 2.6 hPa (Collins et al. 2006b). The land component (Oleson et al., 2004; Bonan and Levis, 2006; Dickinson et al., 2006) shares the same horizontal resolution as the atmospheric component. The ocean model, called Parallel Ocean Program (POP), is a descendant of Bryan–Cox–Semtner models and its dynamics are described by the primitive equations, using the hydrostatic and the Boussinesq approximations (Semtner and O'Brien, 1986; Smith and Gent, 2004). The ocean model uses a non-regular grid with numerical poles over Antarctica and Greenland leading to a resolution of approximately $3.6^\circ \times 1.8^\circ$ with a refinement of up to 0.9° in the tropics. The ocean model has 25 irregularly spaced levels to 5000 m depth. In the upper ocean (0–1000 m) 16 levels are used, with eight levels in the first 100 m. The sea ice model is a state-of-the-art dynamic–thermodynamic model. It incorporates an elastic–viscous–plastic ice rheology and five categories of ice thickness distributions (Briegleb et al., 2004; Holland et al., 2006). The sea ice component has the same horizontal resolution as the ocean.

CCSM3 is used to perform a control simulation and a series of sensitivity experiments with a freshwater discharge in the North Atlantic. In all experiments, external forcing parameters (greenhouse gas concentrations, total solar irradiance, and orbital parameters) are kept constant at 1990 A.D. levels. The experiments are branched from a spin-up control experiment of 810 model years that was provided by NCAR (Yeager et al., 2006).

The study is based on five experiments (Table 1): The control experiment (CTRL) is performed for perpetual 1990 A.D. conditions. After the spin-up experiment, the subsequent 180 years are used in the analysis. This control experiment serves as a reference for all sensitivity experiments. The simulated climate of CTRL is discussed in detail in Yeager et al. (2006).

To explore the response of the climate to different strengths of the MOC, we perturbed the model by a uniform freshwater discharge in the North Atlantic (50° – 70° N). Three different maximum perturbation strengths are applied: 0.5 Sv, 1 Sv, and 2 Sv (FC05, FC10 and, FC20), respectively (Fig. 1). Over a period of 100 model years, the freshwater discharge is linearly increased from 0 Sv up to the maximum strength, followed by 100 years of linear decrease back to 0 Sv. After this perturbation the experiments are continued to investigate the further adjustments simulated by the model. As the ocean component is not a free-surface model the freshwater flux has to be simulated by a virtual salt flux similar to Hu et al. (2008). For simplicity we refer to this flux as 'freshwater

Table 1

Summary of control and sensitivity experiments. F_{\max} denotes the peak freshwater flux input into the North Atlantic (50° – 70° N), "Comp." indicates a globally uniform salt flux that compensates the freshwater flux into the North Atlantic to conserve the global mean salinity.

Name	F_{\max} [Sv]	Comp.	Duration [model years]
CTRL	None	–	180
FC05	0.5	Yes	580
FC10	1.0	Yes	600
FC20	2.0	Yes	780
FN20	2.0	No	1000

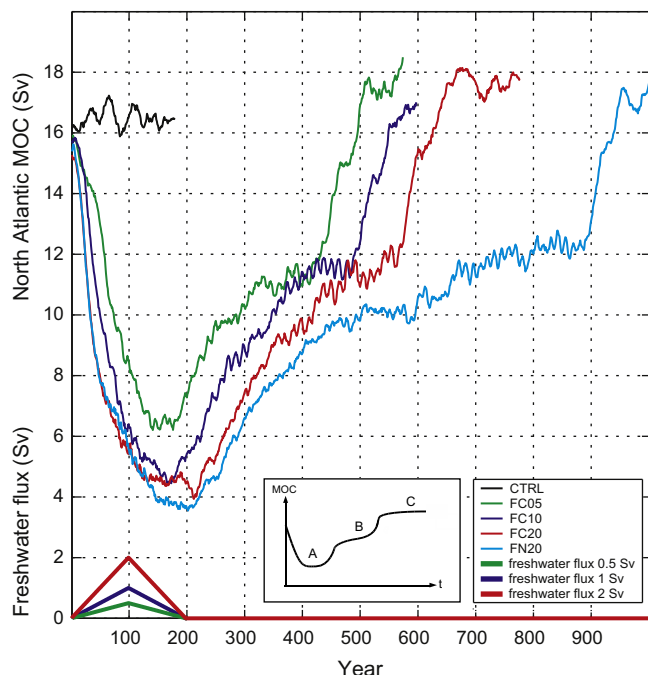


Fig. 1. Response of the North Atlantic maximum meridional overturning circulation to different freshwater forcings into the North Atlantic. Time series is smoothed with a 10-yr running mean. The inset schematically shows the three phases in the evolution of the Atlantic MOC. The freshwater forcing, which is applied to the North Atlantic (50° – 70° N) over 200 years, is shown at the lower left corner.

flux'. Salt is uniformly taken out of the uppermost layer of the North Atlantic and evenly distributed to the rest of the ocean surface. This compensation ensures that the global salt content remains constant. Note that this approach is routinely used in freshwater experiments (Vellinga and Wood, 2002; Knutti et al., 2004), but also exhibits specific problems when far-field effects are being studied (Stocker et al., 2007). To test this specific application of the freshwater flux in the model, an additional experiment is carried out. For this experiment (FN20), a similar approach is used as for FC20, but the salt taken out of the North Atlantic is not redistributed to the rest of the ocean. A detailed analysis of the implications of salt compensation is given in Stocker et al. (2007).

The analysis in this paper focuses on the FC20 experiment, as the experiments forced with a weaker freshwater flux show qualitatively similar results but with less pronounced impacts. In case of differences between the sensitivity experiments, relevant processes are discussed separately.

3. Results

The response of the maximum MOC to the freshwater forcing shows a strong reduction followed by a two-phase recovery after the freshwater forcing is deactivated (Fig. 1). To gain insight in the underlying processes we subdivided the recovery of the MOC into three phases (Fig. 1, inset). After a rapid decline caused by the freshwater forcing, the MOC reaches a minimum of about 4 Sv in FC20 (5 Sv in FC10, 6 Sv in FC05, respectively). The minimum, denoted as phase A, is reached within 150–200 years and lasts for about 50 yr. The transition from phase A to B depends on the strength of the earlier freshwater forcing, which generates different salt gradients between the forced area and its surroundings. The effect is also evident when comparing both experiments forced by 2 Sv, i.e., FC20 and FN20. Experiment FN20 exhibits less saline surface waters outside the perturbed area than

FC20, leading to a smaller salt gradient in FN20. This is the reason for the longer transition from A to B in experiment FN20.

Phase B is characterized by a plateau at about 11 Sv irrespective of the prior forcing. The length of this phase depends again on the strength of the forcing. It is characterized by sea ice melting south of Cape Farewell in the region of the subpolar gyre (SPG) due to the incipient heat transport by the conveyor. Subsequently, the MOC rapidly increases to a state, which is ~ 1 Sv stronger than the initial strength in the CTRL experiment. This state is denoted as phase C (Fig. 1).

In the following we focus on the density in the North Atlantic which determines processes associated with the MOC. Then, the maximum response of the MOC to the freshwater forcing (phase A) is compared with the CTRL experiment. To investigate the resumption process the phases are compared with the prior phase.

3.1. The maximum response of the MOC

To investigate the maximum response of the MOC we compare mean quantities over phase A with those of the CTRL experiment. The meridional overturning cell weakens from approximately 16.5 Sv to 4 Sv in the FC20 experiment. In the CTRL experiment, warm and saline water from the subtropical Atlantic flows northward to the subpolar region and sinks at latitudes between 40° N and 60° N (Fig. 2a). Reaching a depth of 2000 m water masses move then southward as North Atlantic Deep Water. This circulation is reorganized during phase A in all experiments: the overturning circulation is active between 0° and 35° N in phase A and only reaches depths of 1500 m (as shown for FC20 in Fig. 2c). As a consequence of the weaker and shallower overturning cell, water masses of the Antarctic Bottom Water move further northwards and expand up to 2000 m depth.

Associated with the changes of the circulation, the northern North Atlantic is substantially colder in phase A than in the CTRL experiment (Fig. 2b and d) and the sea ice strongly extends to the south in winter and summer (Fig. 3). The sea surface temperature (SST) of phase A in FC20 is decreased by approximately 6° C in the entire North Atlantic with two minima in the GIN and Labrador Seas, which is in good agreement with other model studies (Stouffer et al., 2006). Note that the GIN Seas are covered by sea ice during the entire year.

One striking feature is the positive SST anomaly off the east coast of North America around 42° N (Fig. 2d). This SST increase is caused by changes in the SPG and the subtropical gyre in the North Atlantic. Comparing phase A of experiment FC20 with CTRL shows that the strength of the SPG decreases by 20 Sv, whereas the strength of the subtropical gyre remains constant in its center and intensifies at its northern boarder at 42° N (Fig. 4a and c). The western boundary current of the North Atlantic becomes shallower and intensifies. These changes in gyre circulation can be traced back to an increase of sea ice and a positive sea level pressure (SLP) anomaly. The sea ice cover shelters the SPG from the direct influence of the wind stress and, hence, the SPG weakens. Moreover, the increase of sea ice cools the atmosphere and leads to a positive SLP anomaly, which expands from the North American continent to continental Europe (not shown). This SLP anomaly, in turn, causes a wind stress curl anomaly which intensifies the subtropical gyre and weakens the SPG. Additionally, the line of zero wind stress curl, the separation between the two gyres, moves ~ 250 km northward. Water masses of the subtropical gyre are warmer than the SPG. Thus, the northward displacement leads to a strong positive SST anomaly, which is found in FC20 and all other experiments. Note that such a warming is also found in similar experiments with a model of intermediate complexity but with less amplitude

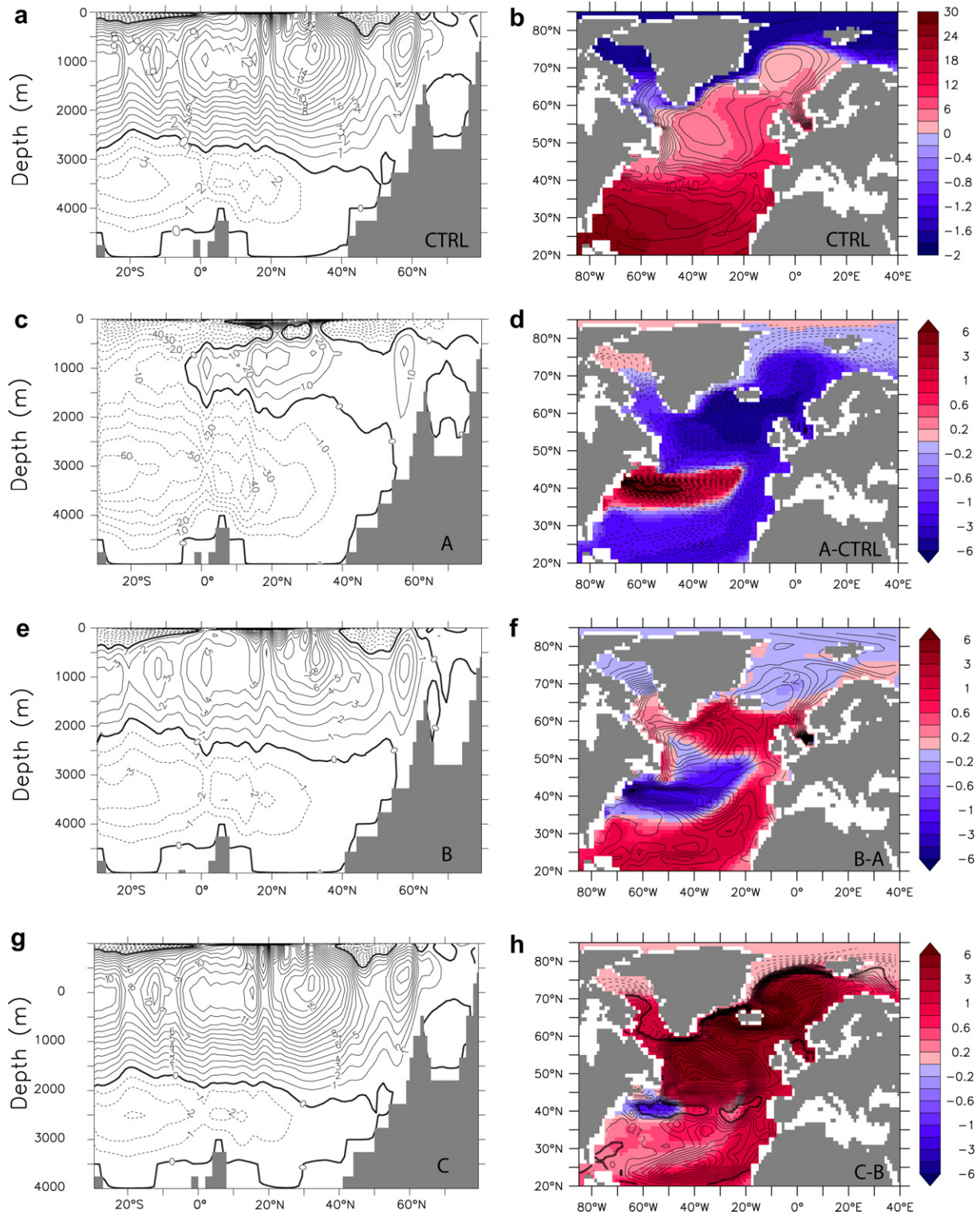


Fig. 2. Mean Atlantic meridional overturning circulation (left panels, contour interval 1 Sv) and sea surface temperatures and their anomalies (shading in °C), as well as sea surface density (contours) in the North Atlantic (right panels): (a, b) CTRL experiment, (c, d) phase A, (e, f) phase B, and (g, h) phase C. Note that panels (d), (f), and (h) show differences for the previous phase, i.e., (d) A minus CTRL, (f) B minus A, and (h) C minus B. Contour interval is 1 Sv for the left panels and 0.5 kg m^{-3} for the right panels.

(Stocker et al., 2007). In the subtropics the FC20 experiment shows a cold tongue, which follows the subtropical gyre on its eastern boundary to the Caribbean (Fig. 2d). This is due to the enhanced subtropical gyre, which advects cold North Atlantic water to lower latitudes.

To further understand the impact of the surface freshwater forcing we investigate surface density changes and separate them with respect to surface salinity and SST changes. The contribution of salinity S and potential temperature θ to the change in surface density ρ can be estimated by

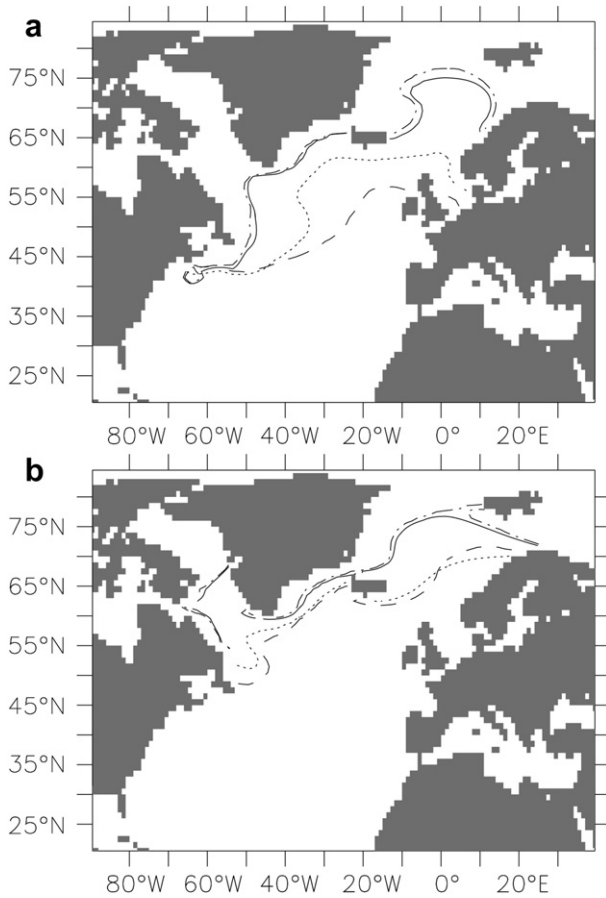


Fig. 3. The mean 10% sea ice concentration fraction for (a) winter (DJFM) and (b) summer (JJAS) during the CTRL experiment (solid), phase A (dashed), B (dotted), and C (dashed-dotted) of the experiment FC20.

$$\frac{\partial \rho}{\partial t} = \rho_0 \left(-\alpha \frac{\partial \theta}{\partial t} + \beta \frac{\partial S}{\partial t} + \dots \right), \quad (1)$$

where t is the time, $\alpha = -(1/\rho)(\partial\rho/\partial\theta)$ is the linear thermal expansion coefficient of sea water, and $\beta = (1/\rho)(\partial\rho/\partial S)$ is the linear coefficient for salinity. Higher-order terms are neglected. Fig. 5a and b show the changes in surface density due to surface salinity and temperature changes between CTRL and phase A of FC20 experiment. As expected the salinity contribution causes a strong decrease in surface density in the entire North Atlantic with a maximum over the forcing area. The density change due to the subsequent cooling of the sea surface is positive, but approximately 10 times smaller than the salinity contribution. The temperature contribution is strong in the region south of Iceland, due to the warm water, which was advected by the eastern part of the significantly weaker SPG. The negative SST anomaly (Fig. 2d) leads to a southward extension of the sea ice cover in the North Atlantic in winter and summer (Fig. 3). However, the salinity input due to an increase in sea ice formation is negligible with respect to the freshwater forcing. South of the forcing area the surface density is decreased as freshwater is advected to the tropics by the northward expansion of the subtropical gyre (Fig. 4b). The subtropical gyre transports relatively fresh and cold water masses southward at its eastern boundary. However, due to the northward expansion of the subtropical gyre at 40°N the negative contribution of salt to density is slightly damped, as subtropical water is more saline. The higher SSTs in this region negatively contribute to the density.

The freshening and the induced surface density changes have an impact on the main ventilation areas, i.e., the GIN Seas, Irminger Basin and the central SPG. To illustrate these ventilation processes we use the maximum mixed layer depth, which is associated with the convective layer depth. In the CTRL experiment areas with increased mixed layer depth extend along the eastern coast of Greenland, in the Irminger Basin, and in the central region of the SPG (Fig. 6). In the GIN Seas the mixed layer depth is shallower than at the southern tip of Greenland with a maximum of about 200–300 m suggesting that the ventilation is strongest in the latter region. As expected, the deep water production disappears during phase A in all experiments. Only the convection south of 35°N remains active as indicated by a small increase of the maximum mixed layer depth during phase A of the FC20 experiment. Hence, this region is exclusively responsible for the remaining shallow overturning of about 4–6 Sv. As a consequence the deep western boundary current becomes weaker by about 40%.

3.2. The resumption of the MOC

In this model configuration the resumption of the MOC is a two-phase process starting with a slow transition from Phase A to Phase B and then an abrupt transition from Phase B to C. The two-phase nature of the resumption is a robust result in these experiments and does not depend on the forcing strength and the method (compensation/no compensation; Fig. 1). Thus, we focus our analysis in the following on FC20.

3.2.1. Transition from phase A to B

The transition from phase A to B is characterized by an increase of the MOC to a value of ~ 8 –12 Sv from about year 300–600 in experiment FC20 (Fig. 1). The time behavior is reminiscent of a relaxation process, i.e., $MOC(t) \sim (1 - e^{-t/\tau})$, with the characteristic time scale τ of approximately 80, 100, 130, and 200 yrs for experiments FC05, FC10, FC20, and FN20, respectively. Clearly, this intermediate MOC value of ~ 11 Sv is model dependent. Surprisingly, similar critical values ranging from 10 to 12 Sv are also found in other studies (Stocker and Schmittner, 1997; Knutti and Stocker, 2002; Mikolajewicz et al., 2007) investigating the stability of the MOC to increasing greenhouse gases.

In our experiments the transition from phase A to B is characterized by a gradual erosion of the large surface salinity gradient between the forced area and its surroundings, after the freshwater forcing has been set to zero at the end of phase A. The MOC is not only strengthening, but also changes its spatial structure. Fig. 2e shows the meridional cross-section of the Atlantic overturning during phase B. The overturning cell at 60°N is enhanced by approximately 2 Sv compared with phase A. The second overturning cell at 35°N is also increased and extends again to the Southern Hemisphere. This weakens the inflow of Antarctic Bottom Water significantly and restricts it to depths below 2500 m in phase B.

Changes of the ocean circulation have an impact on the SST. The SST of the northern North Atlantic (Fig. 2f) shows a tripole pattern with an increase of up to 2 °C between Greenland and Iceland, a weakening of the positive SST anomaly at 42°N, and an increase over the tropical Atlantic. This tripole pattern is caused by changes of the gyre circulation, which show a strengthening of the SPG by ~ 10 Sv and a southward expansion at its eastern boundary during the transition from phase A to B (Fig. 4c). Note that surface heat fluxes damp the SSTs in the gyre regions (not shown). As 2 °C warm water enters the SPG, the SST of the Irminger Basin is increased and the sea ice cover shifts northwards particularly in winter (Fig. 3a). As a result the SPG region becomes ice free and, therefore, it is exposed to wind stress leading to an additional strengthening of

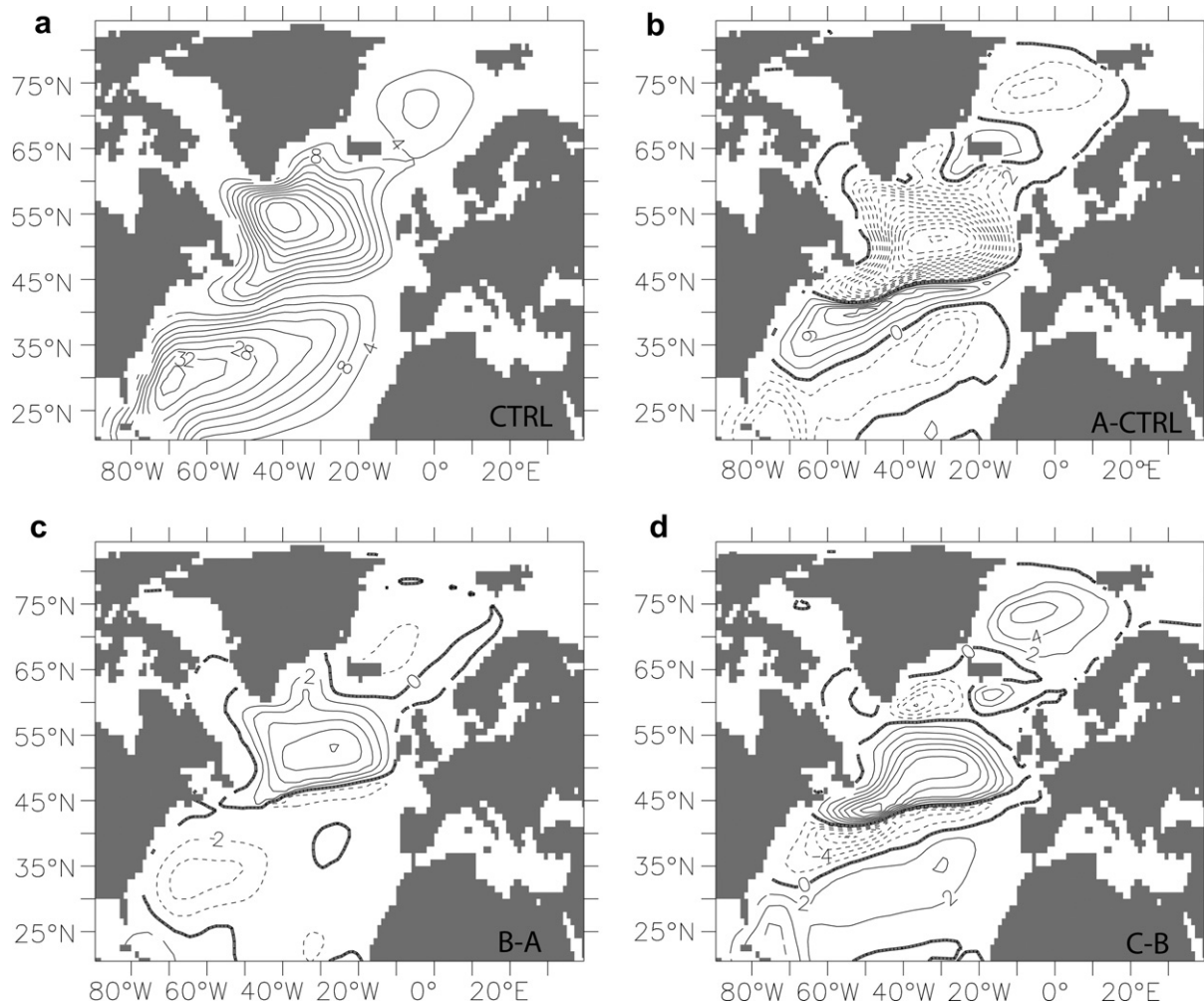


Fig. 4. Barotropic stream function (Sv) and anomaly in experiment FC20: (a) CTRL, (b) A minus CTRL, (c) B minus A, and (d) C minus B. The contour interval is 2 Sv.

the SPG, due to an increase of density by Ekman upwelling in the SPG. In the center of the SPG dense bottom water wells up to the surface. At the surface this bottom water is transported off-center leading to an additional increase of the density of the upper layers. This in turn supports the recovery of the MOC due to a change in the stratification at the edge of the gyre. There, mixing starts at selected grid cells.

The increased SST and the reduced south-to-north salinity gradient (due to the deactivation of the freshwater forcing) change the surface density. The contribution of temperature and salinity to density during phase B (with respect to phase A) is dominated by the back-flow of saltier water masses from the southern ocean (Fig. 5c and d). The temperature contribution is negligibly small despite a mean warming of 1.5 °C to 2 °C in the areas south of Iceland and in the Irminger Basin.

To further understand the slow basin-wide advective process during the transition from phase A to B the ventilation is investigated focusing on the three areas, the North Atlantic around 40°N, the region of the SPG, and the GIN Seas (Fig. 7). Again, the maximum mixed layer depth is used to illustrate the convective activity in the ventilated areas. During the transition from phase A to B the maximum mixed layer depth of the North Atlantic around 40°N (Fig. 7a) exhibits a deepening from ~100 m to ~250 m where the major resumption of the MOC takes place. This behavior is found in all experiments, but with a different strength (FC05 by

10 m, FC10 by 60 m compared to phase A). North of this area in the region of the SPG, we find an oscillation behavior of the maximum mixed layer depth with growing amplitude during phase B (Fig. 7b). This behavior of the maximum mixed layer depth indicates that deep water production restarts but is interrupted by shut downs with a period of about 13 years over the entire phase B. The increase in amplitude is due to an inflow of salty water from low latitudes from cycle to cycle. The velocity of the water masses and therefore the amount of salt per time, which flows into the SPG area, increases due to the enhanced MOC from cycle to cycle. In the GIN Seas, the maximum mixed layer depth increases by ~50 m. However, the maximum mixed layer depth does not oscillate or increase to values similar to the CTRL experiment, as the sea ice cover during the winter (Fig. 3a) and the weak polar gyre (Fig. 4c) inhibit ventilation processes in the GIN Seas.

This oscillation is not unique to the freshwater hosing experiments presented here. A similar oscillation using the same model but a different forcing (no freshwater forcing, but reduced radiative forcing) was found by Yoshimori et al. (2009), where the MOC weakened accidentally from 16 Sv to 11 Sv in transient experiments from 1500 to 2000 AD. Here, we only briefly describe the mechanism of the oscillation as details are given in Yoshimori et al. (2009). In both experimental setups the essential condition is that the GIN is covered by sea ice. The remaining convection mainly occurs in the Irminger Basin. We start our explanation of the

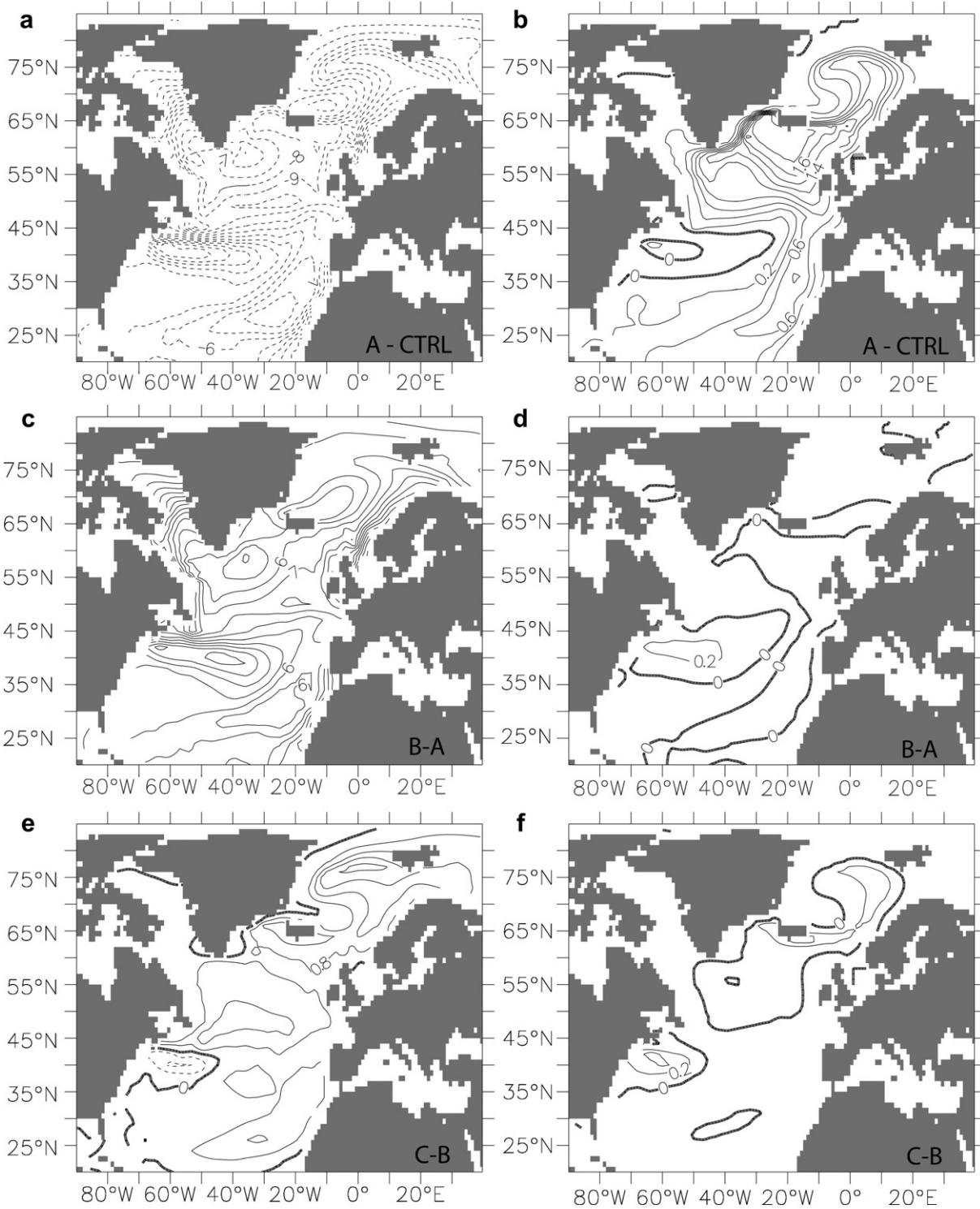


Fig. 5. Changes in surface density in experiment FC20 due to surface salinity changes (left panels) and temperature changes (right panels): (a, b) Phase A minus CTRL, (c, d) B minus A, and (e, f) C minus B. Note that the contour intervals of the temperature contribution to density changes (b, d, f) is 0.2 kgm^{-3} and the contour intervals of the salinity contribution is 1 kgm^{-3} (a, c) and 0.8 kgm^{-3} (e), respectively. Positive values indicate an increase in density and vice versa.

oscillation cycle in the situation of increased surface density in the Irminger Basin. This is accompanied by lower sea surface height and a stronger SPG. While deeper convective activity goes along with a stronger MOC in 4–5 years, the stronger SPG transports fresh Labrador Sea near-surface water to the Irminger Basin. The surface density in the Irminger Basin becomes minimal after 6–8 years of the maximum which in turn results in higher sea surface height,

weaker SPG, and shallower convective activity. This leads to a periodicity of about 13 years. Note that the strength of the SPG seems to be affected by the phase of North Atlantic Oscillation and the westerlies (Raible et al., 2001; Raible et al., 2004; Luksch et al., 2005). Positive NAO tends to be accompanied by a stronger MOC (Yoshimori et al., 2009). Still, the oscillation may be an intrinsic feature of the model used.

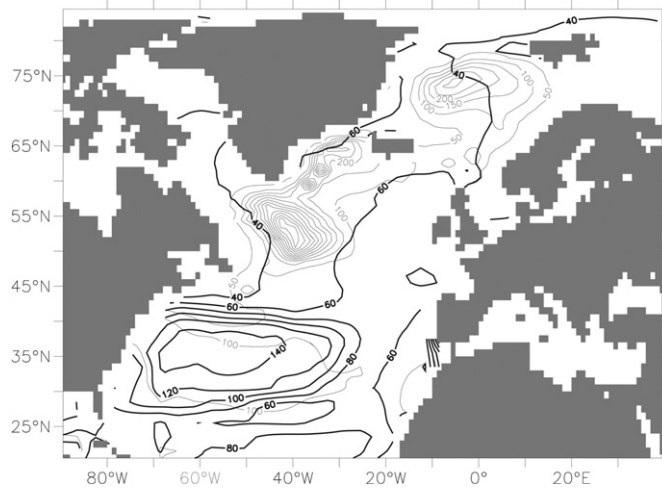


Fig. 6. Maximum mixed layer depth (m) of the CTRL experiment (thin contours, interval 50 m) and phase A of the FC20 experiment (bold contours, interval 20 m).

3.2.2. The transition from phase B to C

The characteristic of the transition from phase B to C is entirely different from the basin-wide advective process of A to B, showing an abrupt increase from 11 Sv to 17.5 Sv which is completed within 60–80 years. This suggests that different processes are involved in the transition from phase B to C. The meridional cross-section of the Atlantic overturning during phase C (Fig. 2g) is similar to the CTRL experiment (Fig. 2a) with two major sinking zones at 40°N and 60°N. The SST increases by up to 7 °C in the GIN Seas in phase C compared with phase B (Fig. 2h). The sea ice cover is strongly

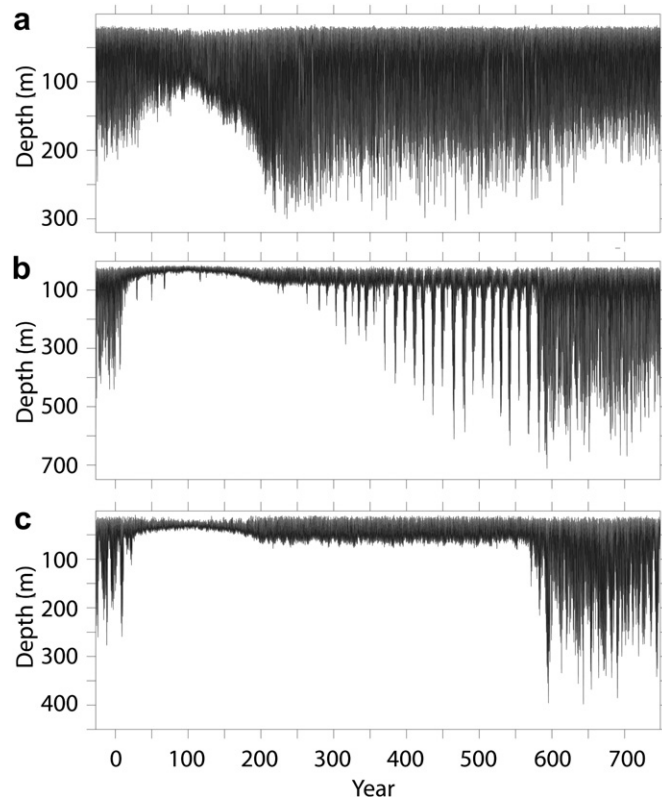


Fig. 7. Time series of maximum mixed layer depth (m) of FC20: (a) Atlantic averaged over the area 35°–40°N and 70°–30°W, (b) over the SPG and, (c) over the GIN Seas.

reduced and reaches a similar extension as the CTRL experiment in both seasons (Fig. 3). The strengths of the SPG and the polar gyre are enhanced by 12 Sv and 6 Sv, respectively (Fig. 4d). As both gyres are ice free and thus exposed to wind stress the convection is further intensified by Ekman upwelling (not shown). The enhanced SPG transports warm and salty water masses at its eastern boundary northwards, which assists in increasing the SST, melting the sea ice and starting the ventilation in the GIN Seas. Again, the density increase is dominated by the salinity rather than temperature changes as illustrated in Fig. 5e and f.

To assess the reason for the abruptness of the MOC increase we now focus on the time behavior of sea ice cover, sea surface density, salinity, and temperature over the GIN Seas and the eastern boundary of the SPG. The area of sea ice cover over the GIN Seas is reduced from a maximum of about $2.5\text{--}0.6 \times 10^{12} \text{ m}^2$ (Fig. 8). Moreover, the annual sea ice area of about $2 \times 10^{12} \text{ m}^2$ is reduced to $0.6 \times 10^{12} \text{ m}^2$. The sea ice over the GIN Seas already gradually retreats during phase B (starting around year 300 in FC20; Fig. 8). The major retreat is found in the summer season and it is restricted to the Norwegian Sea (Fig. 3) where warm water masses enter through the Scotland–Iceland ridge. This gradual penetration of warm and salty water is essential, as it slowly enhances the surface salinity and therefore the density. To illustrate this we show the time series of the surface density averaged over the GIN Seas (Fig. 9) as well as the vertical cross-section of potential density, salinity, and potential temperature – all averaged over the GIN Seas and the different phases A, B, and C (Fig. 10). Clearly, the destabilization of the water column is evident when comparing the vertical density distribution of phases C and B (Fig. 10a). As expected the salinity plays the important role (Fig. 10b), whereas the potential temperature (Fig. 10c) only marginally stabilizes the water column.

The time series of the surface density suggests that a threshold is crossed in the transition from B to C (Fig. 9). After reaching a surface density of approximately $\rho = 1024.5\text{--}1025.0 \text{ kg m}^{-3}$, the ventilation processes in the GIN Seas restart (Fig. 7c). FN20 differs from experiments with salt compensation

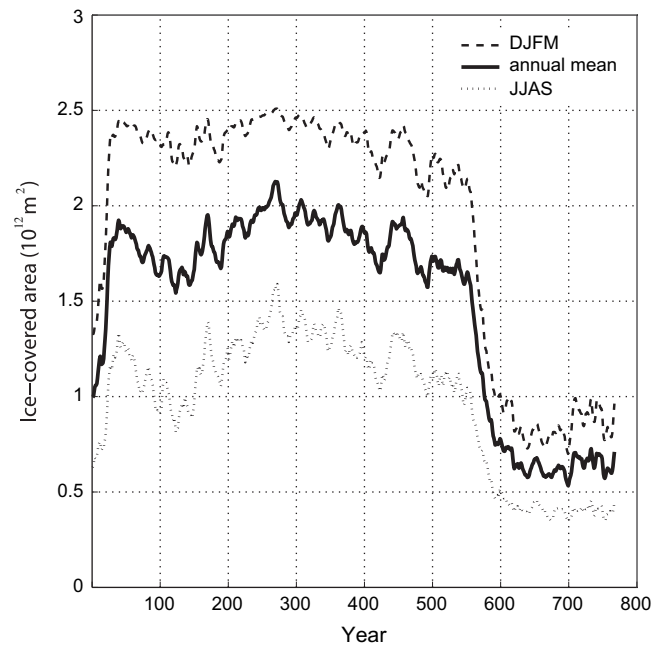


Fig. 8. Time series of the annual, the winter (DJFM), and the summer (JJAS) sea ice cover of the GIN Seas in experiment FC20. Time series are smoothed with a 10-yr running mean.

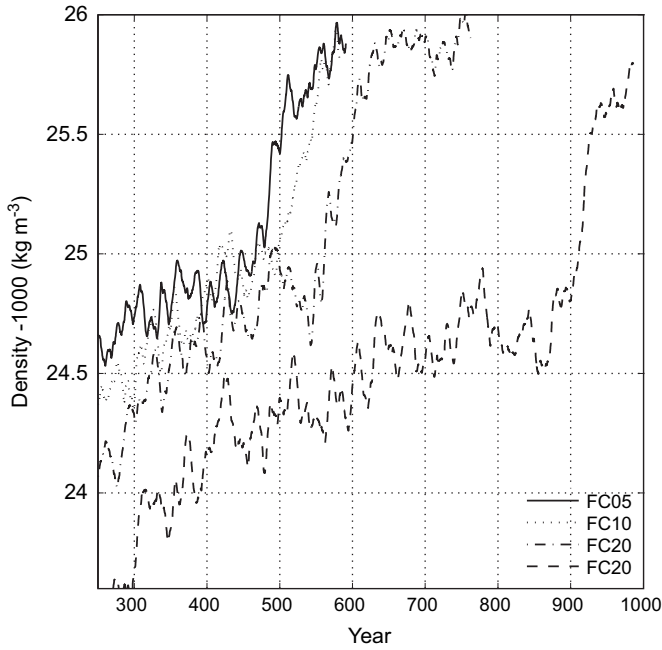


Fig. 9. Time series of the sea surface density averaged over the GIN Sea during the transition from phase B to C for all experiments. Time series is smoothed with a 10-yr running mean.

(FC05, FC10, and FC20), as it takes about 300 years longer before the density threshold is reached. In all experiments the density increase intensifies immediately after reaching the given threshold. A comparison of Figs. 7 and 8 reveals that the ventilation of the GIN Seas starts at the same time as the fast sea ice retreat takes place. The deepening of the mixed layer of the GIN Seas starts a decade before the oscillation stops. Once convection is restarted, warm water from the south increases the SST and causes a rapid ice melting (Fig. 8).

The enhanced polar gyre leads to an increased upwelling of relatively warm and salty water (Fig. 11). The heat supports further ice melting and the enhanced salinity (Fig. 11c) increases the surface density resulting in a positive feedback for deep water production and a rapid increase in SST in the GIN Seas up to 7 °C in several decades follows (Fig. 11d). However, the effects are not restricted to the GIN Seas. Fig. 11a and b illustrate the situation of the flow along the eastern boundary of the SPG into the GIN Seas. Due to the activation of the deep water ventilation, approximately 2 psu saltier water from North Atlantic enters the Iceland–Scotland ridge and further enhances the buoyancy loss in the Norwegian Sea 20 years after the ventilation starts. Thus, this enhanced surface salinity is transported via the East Greenland current to the Irminger Basin which helps stabilize the ventilation processes in the SPG region (Fig. 7b). The resumption of deep water production and therefore a stronger overturning causes a current of relatively warm water at the surface from lower latitudes entering the Nordic Seas. This in turn restarts the outflow of dense cold water through the Denmark Strait and over the Iceland–Scotland ridge. To illustrate this Fig. 12 shows the velocity averaged over the Iceland–Scotland ridge (300 m to the bottom) for the experiment FC20. This velocity increases by a factor of 6 from the transition B to C. Thus, these water masses are exported as Atlantic bottom water.

The rapid transition from phase B to C causes not only a reorganization of the SST, but also of the surface air temperature (SAT) mainly in the North Atlantic. Most of the abrupt warming is found over the GIN Seas as the Hovmoeller diagram of SAT, zonally

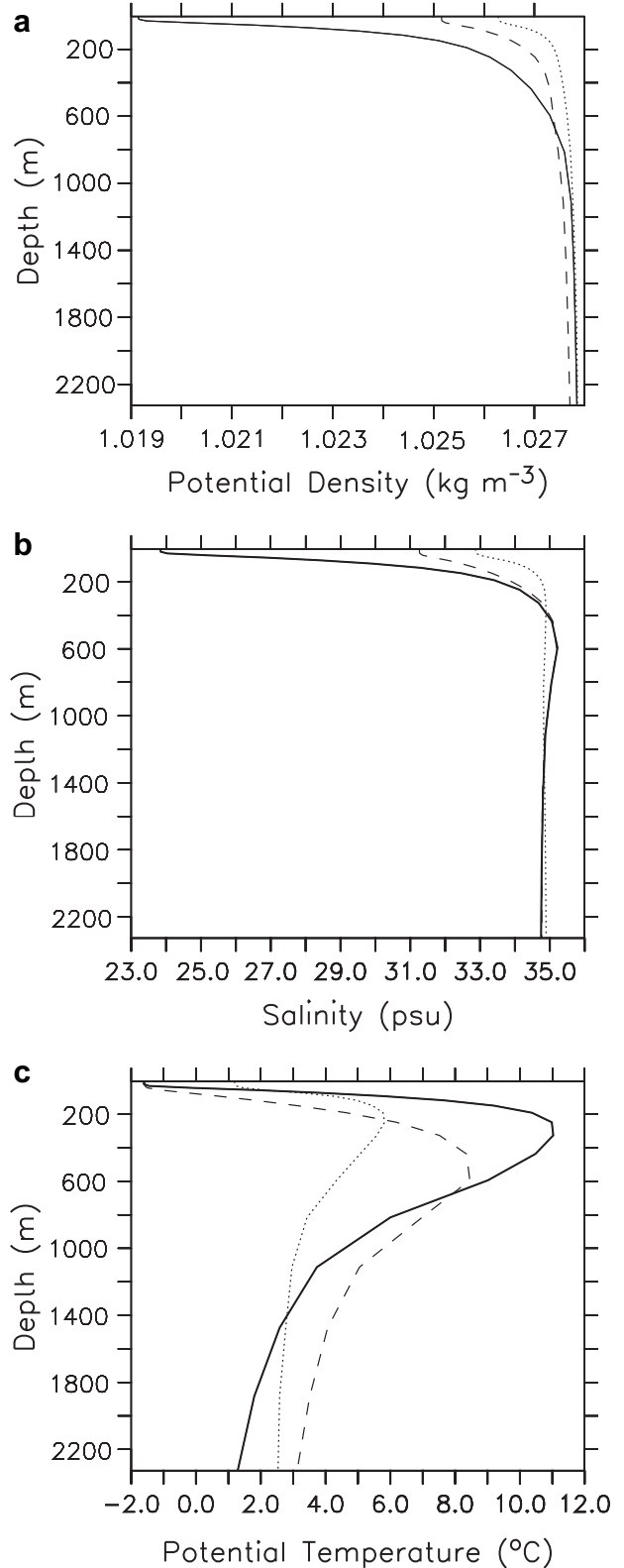


Fig. 10. Vertical profiles of (a) potential density, (b) salinity and (c) potential temperature averaged over the GIN Seas (area shown in the inset Fig. 11c) during the phase A (solid), B (dashed), and C (dotted) of the experiment FC20.

averaged over the Atlantic, shows for experiment FC20 (Fig. 13). However this has implications also for Greenland temperature (Fig. 14). We clearly find a warming of approximately 7 °C within 60–80 years for the FC20 experiment. In terms of amplitude this

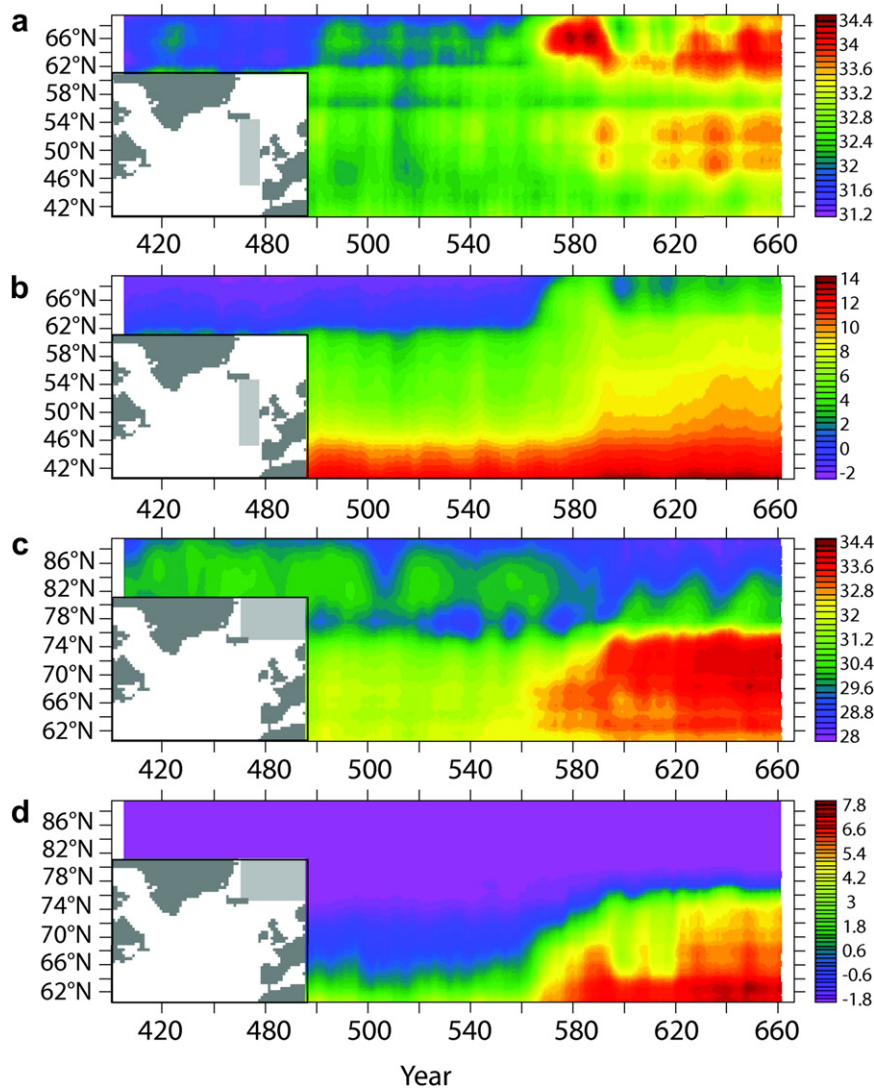


Fig. 11. Hovmoeller diagram of (a, c) the sea surface salinity (psu) and (b, d) sea surface temperature ($^{\circ}\text{C}$) during the transition from phase B to C for experiment FC20. The light gray shading of the insets represents the two areas where the variables are averaged.

increase is in the range of D/O events as proxy data suggests (Huber et al., 2006) but the speed of the change may be severely underestimated (Steffensen et al., 2008).

4. Summary and discussion

The MOC is an important component of the climate system varying on decadal to multi-decadal time scales (Stocker (2000); Kuhlbrodt et al., 2007). A better understanding of the processes driving such changes of MOC is still needed to further decrease the uncertainty of future MOC responses under global warming (Stouffer et al., 2006) as well as to help in the interpretation of proxy data (EPICA Community Member, 2006; Fischer et al., 2008). Here, we contribute to this by presenting sensitivity experiments applying different freshwater perturbations to the North Atlantic and focusing on the resumption process.

The results from these experiments exhibit a two-step resumption process which is independent of the freshwater forcing. The processes involved in the two steps are a slow basin-wide advective process and a subsequent abrupt convective process.

- The slow basin-wide advective process is mainly oceanic and occurs on a characteristic time scale τ . This time scale is found to be dependent on the freshwater forcing. The strong meridional density gradient established by the freshwater forcing is slowly reduced by advection and mixing leading to gradual strengthening of the MOC. The subtropical gyre provides warm and salty water which reduces the sea ice in the North Atlantic. However, the GIN Seas are still covered with sea ice. During this first step of the resumption the MOC starts to oscillate. Within this oscillation, pulses of cold and freshwater from the GIN Seas are transported to the SPG via the Denmark Strait. However, the steady inflow of warm and salty water from the subtropical gyre proceeds until a surface density threshold is reached north of Iceland.
- The crossing of this threshold starts in the second phase of the resumption process and is initiated by convection. The ventilation restarts and enhances the transport of warm and saltier water into the GIN Seas via the Norwegian Current. This melts the sea ice over the GIN Seas. Additionally, the polar gyre strengthens and brings relatively warm and salty water to the surface via Ekman transport, which in turn further enhances

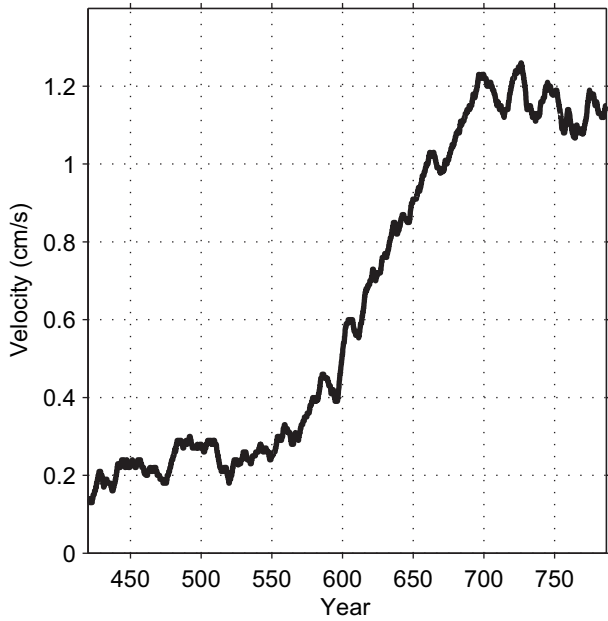


Fig. 12. Time series of velocity over the Iceland–Scotland ridge for the FC20 experiment. The velocity is averaged from 300 m to the bottom.

the overturning due to the geostrophic adjustment caused by the increased density. This positive feedback is responsible for the abrupt warming in the GIN Seas. The oscillation observed during the first transition step is interrupted, because salty and relatively warm water enters via Denmark Strait the Irminger Sea.

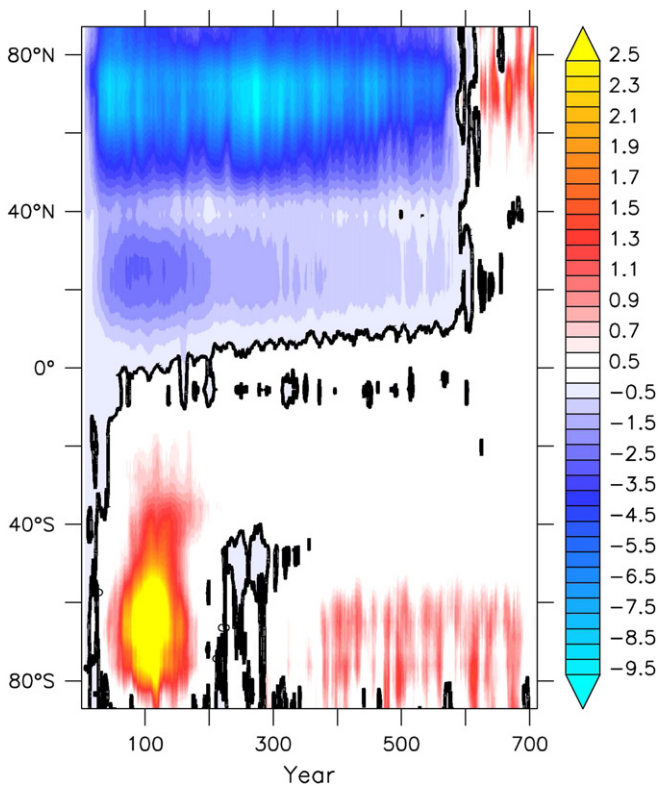


Fig. 13. Hovmoeller diagram of Atlantic surface air temperature anomalies (°C) averaged over 70°W–50°E. The figure illustrates the differences between FC20 and CTRL; the black line indicates 0 °C.

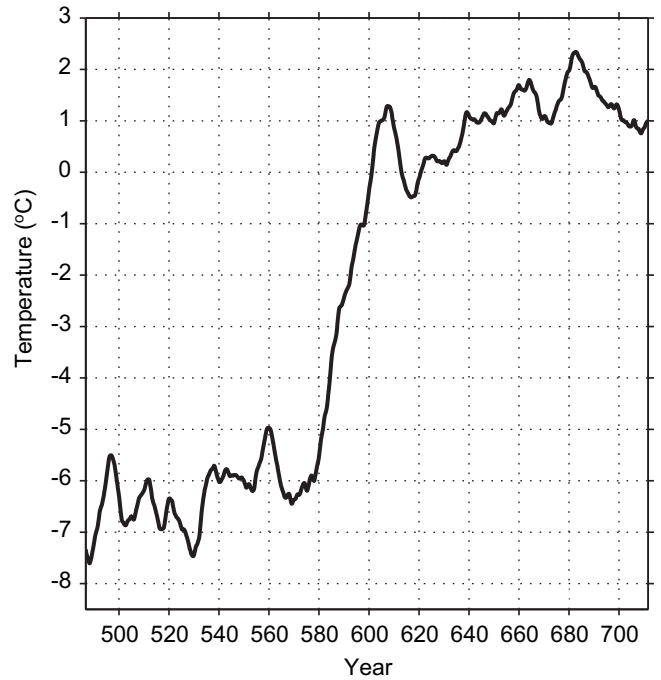


Fig. 14. Time series of Greenland surface air temperature anomalies (°C) focusing on the transition from phase B to C. The surface air temperatures are averaged over 60°–10°W and 65°–75°N. The figure illustrates the differences between FC20 and CTRL. The time series is smoothed with a 10-yr running mean.

Our resumption process is to some extent similar to that found in a recent study by Hu et al. (2008), who uses the same model family, but at a higher resolution. They found a gradual increase of the MOC in all experiments, similar to our first step – however, an abrupt change is not simulated. Closing the Bering Strait leads to a delay of the resumption of the MOC in their simulations. Interestingly, the response of the MOC in their present-day simulation with closed Bering Strait and an LGM simulation is similar. This suggests that our two-step resumption process may be delayed in a simulation under LGM conditions. Moreover, Kleinen et al. (2009) and Otto-Bliesner and Brady (2010) showed that the sensitivity to the location of the freshwater forcing is low. Given this we conclude that our results, in particular the abrupt change from phase B to C could help in a better understanding of the mechanisms of D/O events.

Acknowledgments

This work is supported by the National Centre for Competence in Research (NCCR) on Climate funded by the Swiss National Science Foundation. Experiments are carried out on the IBM SP4 at the Swiss National Computing Centre in Manno, Switzerland and on a local Linux cluster. Constructive comments by three reviewers have helped improve this paper considerably.

References

Barker, S., Diz, P., Vautravers, M.J., Pike, J., Knorr, G., Hall, I.R., Broecker, W.S., Wallace, S., 2009. Interhemispheric Atlantic seesaw response during the last deglaciation. *Nature* 457, 1097–1102.
 Blunier, T., Chappellaz, J., Schwander, J., Dällenbach, A., Stauffer, B., Stocker, T.F., Raynaud, D., Jouzel, J., Clausen, H.B., Hammer, C.U., Johnsen, S.J., 1998. Asynchrony of Antarctic and Greenland climate change during the last glacial period. *Nature* 394, 739–743.

- Bonan, G.B., Levis, S., 2006. Evaluating aspects of the community land and atmosphere models (CLM3 and CAM3) using a dynamic global vegetation model. *J. Clim.* 19, 2290–2301.
- Bond, G., Broecker, W., Johnsen, S., McManus, J., Labeyrie, L., Jouzel, J., Bonani, G., 1993. Correlations between climate records from North Atlantic sediments and Greenland ice. *Nature* 365, 143–147.
- Briegleb, B.P., Bitz, C.M., Hunke, E.C., Lipscomb, W.H., Holland, M.M., Schramm, J.L., Moritz, R.E., 2004. Scientific Description of the Sea Ice Component in the Community Climate System Model. Version 3. National Center for Atmospheric Research, Boulder, CO.
- Collins, W.D., Bitz, C.M., Blackmon, M.L., Bonan, G., Bretherton, C.S., Carton, J.A., Chang, P.C., Henderson, T.B., Kiel, J.T., Large, W.G., McKenna, D.S., Santer, B.D., Smith, R.D., 2006a. The community climate system model: CCSM3. *J. Clim.* 19, 2122–2143.
- Collins, W.D., Rasch, P.J., Boville, B.A., Hack, J.J., McCaa, D.L., Williamson, D.L., Briegleb, C.M., Bitz, C.M., Lin, S.J., Zhang, M., 2006b. The formulation and atmospheric simulation of the community atmosphere model: CAM3. *J. Clim.* 19, 2144–2161.
- Dansgaard, W., Johnsen, S.J., Clausen, H.B., Dahl-Jensen, D., Gundestrup, N.S., Hammer, C.U., Hvidberg, C.S., Steffensen, J.P., Sveinbjörnsdóttir, A.E., Jouzel, J., Bond, G., 1993. Evidence for general instability of past climate from a 250-kyr ice-core record. *Nature* 364, 218–220.
- De Vries, P., Weber, S.L., 2005. The Atlantic freshwater budget as a diagnostic for the existence of a stable shut down of the meridional overturning circulation. *Geophys. Res. Lett.* 32.
- Dickinson, R.E., Oleson, K.W., Bonan, G., Hoffman, F., Thornton, P., Vertenstein, M., Yang, Z.-L., Zeng, X., 2006. The community land model and its climate statistics as a component of the community climate system model. *J. Clim.* 19, 2302–2324.
- Dijkstra, H.A., 2005. *Nonlinear Physical Oceanography*, second ed. Springer, 532 pp.
- EPICA Community Member, 2006. One-to-one coupling of glacial climate variability in Greenland and Antarctica. *Nature* 444, 195–198.
- Fischer, H., Behrens, M., Bock, M., Richter, U., Schmitt, J., Loulergue, L., Chappellaz, J., Spahni, R., Blunier, T., Leuenberger, M., Stocker, T.F., 2008. Changing boreal methane sources and constant biomass burning during the last termination. *Nature* 452, 864–867.
- Goosse, H., Renssen, H., Selten, F.M., Haarsma, R.J., Opsteegh, J.D., 2002. Potential causes of abrupt climate events: a numerical study with a three-dimensional climate model. *Geophys. Res. Lett.* 29, 1860–1864.
- Holland, M.M., Bitz, C.M., Hunke, E.C., Lipscomb, W.H., Schramm, J.L., 2006. Influence of the sea ice thickness distribution on polar climate in CCSM3. *J. Clim.* 19, 2398–2414.
- Hu, A., Otto-Bliesner, B., Meehl, G.A., Han, W., Morrill, C., Brady, E.C., Briegleb, B., 2008. Response of thermohaline circulation to freshwater forcing under present-day and LGM conditions. *J. Clim.* 21, 2239–2258.
- Huber, C., Leuenberger, M., Spahni, R., Flückiger, J., Schwander, J., Stocker, T.F., Johnsen, S., Landais, A., Jouzel, J., 2006. Isotope calibrated Greenland temperature record over Marine Isotope Stage 3 and its relation to CH₄. *Earth Planet. Sci. Lett.* 243, 504–519.
- Kleinen, T., Osborn, T.J., Briffa, K.R., 2009. Sensitivity of climate response to variations in freshwater hosing location. *Ocean Dyn.* 59, 509–521.
- Knorr, G., Lohmann, G., 2003. Southern Ocean origin for the resumption of Atlantic thermohaline circulation during deglaciation. *Nature* 424, 532–536.
- Knutti, R., Flückiger, J., Stocker, T.F., Timmermann, A., 2004. Strong hemispheric coupling of glacial climate through freshwater discharge and ocean circulation. *Nature* 430, 851–856.
- Knutti, R., Stocker, T.F., 2002. Limited predictability of the future thermohaline circulation close to an instability threshold. *J. Clim.* 15, 179–186.
- Knutti, R., Stocker, T.F., Wright, D.G., 2000. The effects of subgrid-scale parameterizations in a zonally averaged ocean model. *J. Phys. Oceanogr.* 30, 2738–2752.
- Kuhlbrodt, T., Griesel, A., Montoya, M., Levermann, A., Hofmann, M., Rahmstorf, S., 2007. On the driving process of the Atlantic meridional overturning circulation. *Rev. Geophys.* 45 RG2001.
- Liu, Z., Otto-Bliesner, B.L., He, F., Brady, E.C., Tomas, R., Clark, P.U., Carlson, A.E., Lynch-Stieglitz, J., Curry, W., Brook, E., Erickson, D., Jacob, R., Kutzbach, J., Cheng, J., 2009. Transient simulation of last deglaciation with a new mechanism for Bølling–Allerød warming. *Nature* 325, 310–314.
- Longworth, H., Marotzke, J., Stocker, T.F., 2005. Ocean gyres and abrupt change in the thermohaline circulation: a conceptual analysis. *J. Clim.* 18, 2403–2416.
- Luksch, U., Raible, C.C., Blender, R., Fraedrich, K., 2005. Cyclone track and decadal Northern Hemispheric regimes. *Meteorol. Z.* 14, 747–753.
- Manabe, S., Stouffer, R.J., 1995. Simulation for abrupt climate change induce by freshwater input to the North Atlantic Ocean. *Nature* 378, 165–167.
- McManus, J.F., Francois, R., Gherardi, J.-M., Keigwin, L.D., Brown-Leger, S., 2004. Collapse and rapid resumption of Atlantic meridional circulation linked to deglacial climate changes. *Nature* 428, 834–837.
- Mikolajewicz, U., Groger, M., Maier-Reimer, E., Schurgers, G., Vizcaino, M., Winguth, A.M.E., 2007. Long-term effects of anthropogenic CO₂ emissions simulated with a complex earth system model. *Clim. Dyn.* 28, 599–633.
- Oleson, K.W., Dai, Y., Bonan, G., Bosilovich, M., Dickinson, R., Dirmeyer, F., Hoffman, P., Houser, P., Levis, S., Niu, G.-Y., Thornton, P., Vertenstein, M., Yang, Z.-L., Zeng, X., 2004. Technical Description of the Community Land Model (CLM). Tech. rep., NCAR/TN-461+STR. National Center for Atmospheric Research, Boulder, CO, 80307–3000, 174 pp.
- Otto-Bliesner, B.L., Brady, E.C., 2010. The sensitivity of the climate response to the magnitude and location of freshwater forcing: last glacial maximum experiments. *Quat. Sci. Rev.* 29, 56–73.
- Rahmstorf, S., 2002. Ocean circulation and climate during the past 120,000 years. *Nature* 419, 207–214.
- Raible, C.C., Luksch, U., Fraedrich, K., 2004. Precipitation and Northern Hemisphere regimes. *Atmos. Sci. Lett.* 5, 43–55. doi:10.1016/j.atmoscilet.2003.12.001.
- Raible, C.C., Luksch, U., Fraedrich, K., Voss, R., 2001. North Atlantic decadal regimes in a coupled GCM simulation. *Clim. Dyn.* 18, 321–330.
- Rind, D., Russell, G., Sheth, S., Collins, D., Demenocal, P., Teller, T., 2001. Effects of glacial meltwater in the GISS coupled atmosphere-ocean model 2. A bipolar seesaw in Atlantic deep water production. *J. Geophys. Res.* 106, 27355–27365.
- Ruddiman, W.F., McIntyre, A., 1981. The mode and mechanism of the last deglaciation: oceanic evidence. *Quat. Res.* 16, 125–134.
- Rühlemann, C., Mulitza, S., Müller, P.J., Wefer, G., Zahn, R., 1999. Warming of the tropical Atlantic Ocean and slowdown of thermohaline circulation during the last deglaciation. *Nature* 402, 511–514.
- Schmittner, A., Saenko, A.O., Weaver, A.J., 2003. Coupling of the hemispheres in observations and simulations of glacial climate change. *Quat. Sci. Rev.* 22, 659–671.
- Schmittner, A., Weaver, A.J., 2001. Dependence of multiple climate states on ocean mixing parameters. *Geophys. Res. Lett.* 28, 1027–1030.
- Semtner, A.J., O'Brien, J.J., 1986. Finite-difference Formulation of a World Ocean Model. D. Reidel Publishing Company, Norwell, Mass.
- Smith, R., Gent, P., 2004. Reference Manual for the Parallel Ocean Program (POP). Ocean component of the Community Climate System Model (CCSM2.0 and 3.0). Los Alamos National Laboratory, Los Alamos, New Mexico. LAUR-02-2484.
- Steffensen, J.P., Andersen, K.K., Bigler, M., Clausen, H.B., Dahl-Jensen, D., Fischer, H., Goto-Azuma, K., Hansson, M., Johnsen, S.J., Jouzel, J., Masson-Delmotte, V., Popp, T., Rasmussen, S.O., Röthlisberger, R., Ruth, U., Stauffer, B., Siggaard-Andersen, M.-L., Sveinbjörnsdóttir, A.E., Svensson, A., White, J.W.C., 2008. High-resolution Greenland ice core data show abrupt climate change happens in few years. *Science* 321, 680–684.
- Stocker, T.F., 1998. The seesaw effect. *Science* 282, 61–62.
- Stocker, T.F., 2000. Past and future reorganizations in the climate system. *Quat. Sci. Rev.* 19, 301–319.
- Stocker, T.F., Johnsen, S.J., 2003. A minimum thermodynamic model for the bipolar seesaw. *Paleoceanography* 18 (4), 1087.
- Stocker, T.F., Marchal, O., 2000. Abrupt climate change in the computer: is it real? *Proc. Natl. Acad. Sci. USA* 97, 1362–1365.
- Stocker, T.F., Schmittner, A., 1997. Influence of CO₂ emission rates on the stability of the thermohaline circulation. *Nature* 388, 862–865.
- Stocker, T.F., Timmermann, A., Renold, M., Timm, O., 2007. Effects of freshwater compensation on the climate model response in simulations of large changes of the Atlantic meridional overturning circulation. *J. Clim.* 20, 5912–5928.
- Stocker, T.F., Wright, D.G., Broecker, W.S., 1992. The influence of high-latitude surface forcing on the global thermohaline circulation. *Paleoceanography* 7, 529–541.
- Stommel, H., 1961. Thermohaline convection with two stable regimes of flow. *Tellus* 13, 224–241.
- Stouffer, R.J., Yin, J., Gregory, J.M., Dixon, K.W., Spelman, M.J., Hurlin, W., Weaver, A.J., Eby, M., Flato, G.M., Hasumi, H., Hu, A., Jungklaus, J.H., Kamenkovich, I.V., Levermann, A., Montoya, M., Murakami, S., Nawrath, S., Oka, A., Peltier, W.R., Robitaille, D.Y., Sokolov, A., Vettoretti, G., Weber, S.L., 2006. Investigating the causes of the response of the thermohaline circulation to past and future climate changes. *J. Clim.* 19, 1365–1387.
- Vellinga, M., Wood, R.A., 2002. Global climatic impacts of a collapse of the Atlantic thermohaline circulation. *Clim. Change* 54, 251–267.
- Vidal, L., Schneider, R., Marchal, O., Bickert, T., Stocker, T.F., Wefer, Y., 2005. Link between the North and South Atlantic during the Heinrich events of the last glacial period. *Clim. Dyn.* 15, 909–919.
- Wang, Z., 2005. Two climatic states and feedbacks on thermohaline circulation in an Earth system model of intermediate complexity. *Clim. Dyn.* 25, 299–314.
- Wright, D.G., Stocker, T.F., 1991. A zonally averaged ocean model for the thermohaline circulation, part I: model development and flow dynamics. *J. Phys. Oceanogr.* 21, 1713–1724.
- Yeager, S.G., Shields, C.A., Large, W.G., Hack, J.J., 2006. The low-resolution CCSM3. *J. Clim.* 19, 2545–2566.
- Yoshimori, M., Raible, C.C., Stocker, T.F., Renold, M., 2009. Simulated decadal oscillations of the Atlantic meridional overturning circulation in a cold climate state. *Clim. Dyn.* 34, 101–121.